Table 6.19: Sulfate episodes during the WHITEX study, January-February 1987 at Monticello, Utah.

Julian Day 1987	NGS Plume	CD_4
9 – 10	No	—
13 – 15	No	—
17	No	—
19 – 20	No	—
23 – 25	Yes	—
26	No	—
28	Yes	—
30	Yes	—
32	No	—
34 – 35	Yes	Yes
41 – 44	(Yes)	(Yes)
47 – 48	No	—

6.4.4 Summary of Meteorological Analysis of WHITEX Study Period

Table 6.20 summarizes the breakdown of the WHITEX study period into the thirteen time periods, and for each day, the synoptic meteorology, the direction from which the ARL-ATAD trajectory approaches Grand Canyon, the wind direction at three altitudes in Page, the wind speed at 600 meters above ground in Page, and the position of NGS plume material relative to NGS on the basis of the plume centerline (streakline) calculations.

On some days winds are so variable that wind directions cannot be identified. These days are indicated by a dash (- -).

There is considerable wind shear indicated in the Page winds. However, the Page winds are often consistent with the winds derived from the analysis of synoptic weather maps and from the ATAD trajectories.

It is striking to note that NGS plume material is often predicted to be spread over much of the area at the same time. This is due to the wind shear and the variable wind directions exhibited during WHITEX.

6.5 Spatial and Temporal Trends in Sulfates

In this section we analyze the spatial and temporal trends in the measured, sulfate concentrations in the WHITEX study region during January and February 1987. The spatial and temporal trends analysis will also use the measured meteorology and the estimated NGS plume parcel age derived from the measured winds, as well as a spatial eigenvector analysis to make inferences regarding potential contributing sources.

6.5.1 Discussion of Sulfate Time Histories

The time histories of the ammonium sulfate concentrations at all of the WHITEX sites are shown in Figure 4.3. An examination of this figure shows that there are periods of relatively uniform

Table 6.20: Summary of meteorological analysis of WHITEX: synoptic meteorology, backward air mass trajectories, Page upper-level winds, and calculated NGS plume locations.

Time Period	Julian Day	Synoptic Meteorology: Synoptic Category	Winds: Light or Strong	Transport from:	ATAD Trajectory from:	Upper-Level Winds Measured in Page, AZ: Wind Direction 300 m agl	600 m agl	1000 m agl	Wind Speed 600 m	Estimated Location of NGS Plume relative to NGS
1	7	3/4	light	SE	SW	NE	NE	NE	4.5	—
	8	3	strong	NE	NW	NW	NW	NW	5.0	—
2	9	4	strong	NE	N	NE	NE	NE	2.8	SW-S-SE
	10	4	strong	NE-E	NE	N-E-S	NW-NE	NW-NE	2.3	S-SE
	11	4	strong	SE	NE	E	E	E	3.0	S-SW-W
	12	4	light	E	E	E-NW	NE-E-SE	S-E	4.5	W-SW
3	13	4	very light	—	—	SE-S-SW	SE-S	W	3.4	SW-W-NW-NE
	14	4	strong	NE	—	NE-S	N-SE	N-NE-SW	1.6	SW-W-NW
	15	3	strong	NE	—	E-SE	SE-S	SW	5.1	W-NW
	16	3	strong/precip.	N-NE	N	—	No Measurements	—		SW
4	17	3	strong	NE	NE	N-NW-NE	N	N	6.3	S
	18	4	strong	NE	N	NW-SE	N-SW	N	2.9	S-SE-E-NE
	19	4	light	NE?	N	E	NW-NE	NW-NE	7.7	W-NW-E-SE-SW
5	20	3/4	strong	NE	NE	NE-SE	NE-SE-N	NE-N	3.4	W-SW-S
	21	4	light	E-NE	N	W-S	N-NW-E	N-NW	3.9	NE-SW-S-SE
	22	4	light	E	N	SE-S-SW	SE-S-SW	NW-W	2.9	NW-SW-NE-S-SE
6	23	3/4	strong	S	SW	S-NE	S-SW	SW-NW	4.1	N-NW-W-SE
	24	4	light	—	—	NE-S-SW	W-SW	W	6.4	W-NW-E-NE
	25	4	very light	—	NW	SW-S-E	SW-W	W	3.0	NE-N-E-NW
	26	4	strong	E-SE	E	SE-SW-NW	SW-S	W	4.6	N-NE-E
	27	4	light	SE	SE	SW-SE	S-SW	W	4.1	N-NE
	28	1/4	strong	SW	SW	SE-SW-NW	S-SW-W	SW-W	11.4	NW-N-NE-E
7	29	4	strong-light	SE	SW	E-NE	E-NE	SE-NE	4.3	W-E-SW-S
	30	4	strong	S-SE	SW	NE-E	E-SE	S	3.4	W-SW-S-N
	31	3	strong	NE	W	N-E	N	NE-NW	7.4	S-SW-W-NW
	32	4	light	NE	NW	NW-S	NW-W-SW	N-W	3.0	SE-S-SW-NE-E
8	33	4	light	S	SW	SW-S-W	S	W-SW	4.4	N-NE-SE-S-SW
	34	1/4	light	—	—	S-SE-NE	S-NW	SW	3.3	NE-E-SE-S-SW
	35	3/4	strong/precip.	NE	NW	N-NE	N-NE	NE	5.0	S-SE-NE-E-SW
9	36	4	strong	E-NE	NE	NE-E	NE-E-NE	NE	4.0	W-SW-S
	37	4	strong	E-NE	NE-E	N-E-NE	N-NE	NE	4.0	SW
	38	4	light	E	E	NW-E-N	E-NE-E	SW-SE	3.2	W-SW-S-SE
10	39	4	strong	SE	SE	E	E-NE-SE	SE-S	6.2	W-SW
	40	4	light	—	S	NE	SE-S-N	S	3.4	NW-W-SW
11	41	4	light	—	SW	S-NE	S-NE	S-NW	4.8	N-NW-W
	42	4	light	—	SW	NE	NE-E	NW	2.5	SW-W-NW
	43	4	light	—	SW	NE-SE	NE-W	S-W	3.5	SW-W-SE-NW
12	44	4	light	—	W	S-N-NE	W-S-W	W-SW	2.4	W-E-SE-SW-NE
13	45	3/4	strong	N-NW	NW	NW	NW	NW	17.1	SE
	46	4	light	—	W	NW-SE-N	NW-S-N	NW-S	7.7	S-SE
	47	3	strong/precip.	NE	N	NW-N-NE	NW-NE	N-NE	5.2	SW-S-SE
	48	3/4	strong/precip.	NE	N	N-NW-N	NE-NW-N	NE	3.5	SE
	49	4	light	NE	N	N	E	E	2.9	S-SW

(homogeneous), as well as highly nonuniform (non-homogeneous), sulfate concentrations in the WHITEX region. One might suspect that long-range transport from distant SO_2 sources would result in relatively uniform sulfate concentrations, while local mesoscale transport from SO_2 sources within the WHITEX region would cause the highly nonuniform concentrations. Also note the dramatic cleansing of the region after the frontal passages on Days 28 and 45.

The average sulfate sulfur concentrations measured during WHITEX vary from a minimum of 0.165 $\mu g/m^3$ at Hopi Point to a maximum of 0.345 $\mu g/m^3$ at Green River. While the average at Page, AZ, the site closest to NGS is 0.332. The difference between maximum and minimum averages is a factor of 2 and even larger differences exist during episodes. At Green River there are three periods during which sulfate concentrations build up to more than 3 $\mu g/m^3$ of ammonium sulfate. These maxima appear on Julian days 9, 28, and 43. The sulfate concentrations prior to Days 9 and 43 build up to their maximum in less than one day, while the maximum on Day 28 is achieved after a sustained buildup of approximately one week. After the maxima on Days 28 and 43, scavenging and scouring of the pollutant is extremely effective when fronts come through, resulting in measured sulfate minima at this site: ammonium sulfate less than 0.5 $\mu g/m^3$.

In contrast to the Green River trends, the measured sulfate at Hopi Point is considerably lower. Also the sulfate maxima occur at different times except for the common maximum on Day 43. Sulfate maxima at Hopi Point occur on Days 15, 34, and 43. Although sulfate concentrations do rise on the days where maxima occurred at Green River, these concentrations are not as high as those on the other days. Except for Day 43, Hopi Point maxima occur at different times than the Green River maxima.

Page, AZ experienced sulfate concentrations generally between the maxima recorded at Green River and the minima at Hopi Point. However, again, except for the common peak in concentration on Day 43, the sulfate concentration behavior at Page is quite different from that at either Green River or Hopi Point. For example, during the multiday episode that results in a sulfate maximum on Day 28 in Green River, sulfate concentrations in Page decrease.

These variations in space as well as time strongly suggest that the sulfate concentrations at these three locations, all within 300 km of one another, could not have been caused primarily by long-range transport from remote locations such as southern California, southern Arizona or Mexico. If this were the case, the sulfate concentrations would be much more similar at the three sites because after long-range transport, concentrations would be relatively uniform on a 300-km scale. The spatial differences suggest that both Green River and Page are strongly influenced by sources of SO_2 within the region, while Hopi Point is less strongly influenced by these local sources.

Also in Figure 4.3, note the temporal trends in sulfate concentrations at five sites along the Colorado River. From west to east, these sites are Hopi Point, Page, Bullfrog Marina, Hite, and Canyonlands (see Figure 6.1). Minimum sulfate concentrations almost always occur at Hopi Point, while maxima are generally recorded either at Page or Hite. If NGS is a significant source of the sulfate along the Colorado River, one might expect that sulfate concentrations would be highest at Page, which is closest to NGS, and progressively lower at sites more distant. Often this does occur. Yet the data show that sulfate concentrations are occasionally higher in Hite than either Page or Bullfrog, both of which are closer to NGS. Possible explanations for the high concentrations at Hite include the fact that it is at the mouth of a tributary of the Colorado that might be a drainage airflow pathway from the Hunter and Huntington Canyon power plants and other SO_2 sources such as the uncontrolled power plants in Wyoming and Colorado. Hite is southeast of these SO_2 sources and is generally downwind from these sources during the WHITEX experiment. The second explanation for the relatively high concentrations at Hite is that the characteristic transport and dispersion patterns for the area, as influenced by elevated terrain, could cause transport, mixing, and trapping of NGS emissions resulting in higher concentrations at Hite than at Bullfrog.

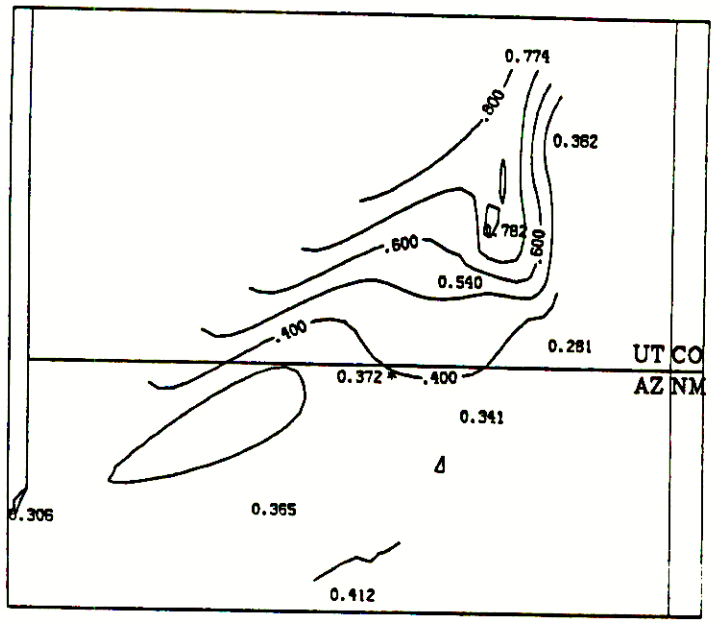

Figure 6.14: Spatial distribution of fine sulfur for JD 8 hour 20.

The temporal trends in sulfate concentration at six sites to the north and east of NGS, including Green River, Canyonlands, Hite, Bullfrog Marina, Monticello, and Mexican Hat can also be compared in Figure 4.3. Again, we see significant spatial inhomogeneity in the region. Concentrations on the same day range between the maxima generally observed in Green River, Mexican Hat, or Hite and the minima generally observed at Monticello and Canyonlands.

6.5.2 Discussion of Spatial Sulfate Patterns

Julian Days 8 and 9

The buildup in sulfate that was measured in Green River and Hite on Julian Days 8 and 9 occurred when winds in the area were from the north half of the compass and when the NGS plume is predicted to be transported generally to the south. Thus, NGS probably is not the most significant source during this episode at these sites unless NGS emissions had earlier been transported into this area. A contour plot of the 12-hour average fine sulfur concentrations beginning on Day 8 hour 20 is shown in Figure 6.14. Spatial sulfur patterns for all 4 12-hour time periods during these two days seem to indicate transport from a source of sulfur north of Green River (perhaps the Jim Bridger and Naughton plants in Wyoming, the Craig and Hayden plants in Colorado an/or the Utah Power and Light plants in central Utah). For receptor site locations on all contour plots see Figure 6.15.

Julian Days 10 through 19

The relatively high concentrations and nonuniformity of WHITEX regional sulfate during the period from Julian Day 10 through 19 may suggest contributions from sources within the region. Winds during this period are extremely variable, thus the NGS plume is predicted to be widely dispersed. The high concentration measured in Mexican Hat on Day 19 occurs when the NGS plume is

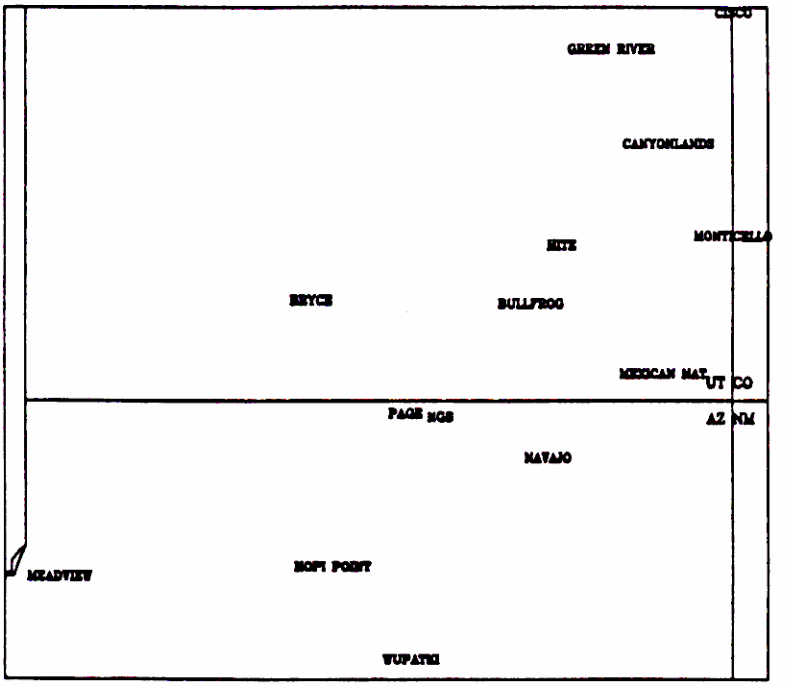

Figure 6.15: Receptor site locations for all concentration contour plots. The name of the site begins at the location.

predicted to be in the area. Yet on the same day, the NGS plume is also predicted to be at Hopi Point in the Grand Canyon (the opposite direction) when a relative sulfate maxima was also measured there. (See the streaklines in Appendix 6H) This behavior can be explained by the highly variable winds and the considerable vertical wind shear. Contour plots of the sulfur measured during these time periods indicate that several sources could have contributed to high sulfur concentrations in the study area. For example The spatial pattern on JD 11 hour 8 (Figure 6.16) indicates that both NGS and sources north of the study area could have been contributors to the sulfate concentrations. The pattern on JD 15 hour 20 (Figure 6.17) suggests NGS as the dominant sulfur source for that time period. The sulfur pattern on JD 19 hour 8 (Figure 6.18) shows sulfur apparently being transported into the area across the eastern and southeastern edges of the study region perhaps from the San Juan and Four Corners Plants. Although during the previous time periods the NGS plume was being transported towards the east, so an alternative explanation might be NGS emissions stagnating and undergoing further oxidation of SO_2 to SO_4 in the complex terrain as the plume was being transported back towards Page. The observed sulfur concentrations could be a combination of both mechanisms.

Julian Days 20 through 28

During the sustained buildup in sulfate from Julian Day 20 to 28, seen most clearly at Green River, Hite, and Bullfrog Marina (Figure 4.3) the streakline analysis predicts that the NGS plume is located in the Green River area. Winds in Page are often from the southwest which could transport NGS emissions to Green River. However, the contour plots of sulfur concentrations during this time period for example the contour plot for JD 21 hour 8 in Figure 6.19 often show highest sulfur concentrations in the northeast portion of study area with concentrations decreasing

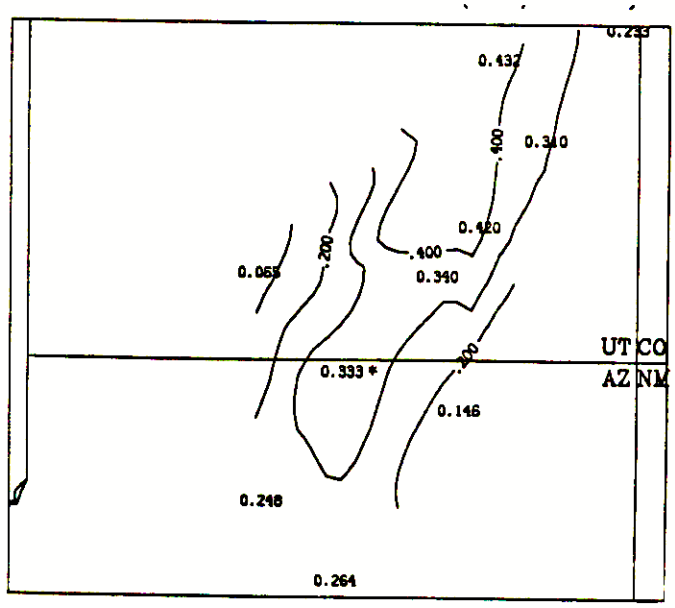

Figure 6.16: Spatial distribution of fine sulfur for JD 11 hour 8.

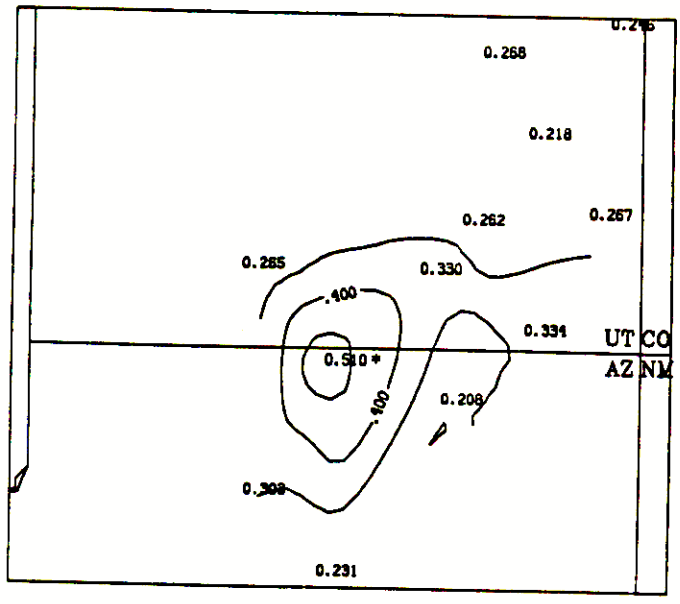

Figure 6.17: Spatial distribution of fine sulfur for JD 15 hour 20.

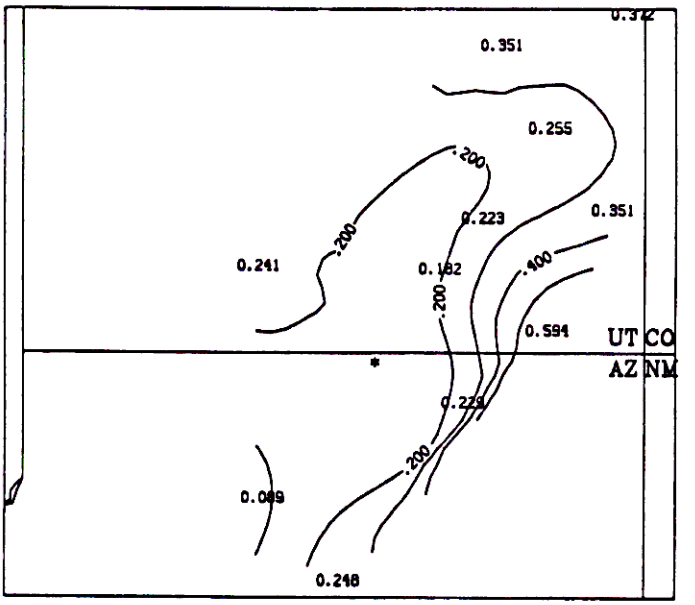

Figure 6.18: Spatial distribution of fine sulfur for JD 19 hour 8.

towards the southwest. This may indicate that the SO_2 emissions from NGS were not sufficiently oxidized to SO_4 until the plume reached the Green River area or that there may also have been some transport of sulfur into the study area from the north.

In the opposite direction from NGS, Hopi Point exhibits low sulfate concentrations, except on Days 23 to 24 when 300-meter winds in Page are from the northeast, which could result in transport directly to Hopi Point. Spatial patterns in the sulfur concentrations during these two days were all similar to that shown for JD 23 hour 8 in Figure 6.20. The concentric rings around Page suggest that emissions from NGS were dispersing outward under somewhat stagnant conditions. At the end of the episode when strong southwesterly winds blow into the WHITEX region, Green River sulfate drops precipitously while Hopi Point concentrations increase. The increase in sulfate at Hopi Point during the period of strong winds suggests transport from different sources.

Julian Days 28 through 35

After relatively uniform concentrations throughout the region on the two days after the frontal passage on Day 28, concentrations again start to build up in a somewhat nonuniform way. Winds are so variable and vertically sheared during this period that NGS emissions are predicted to be dispersed in almost all directions around NGS. The relatively high concentrations at Navajo National Monument and at Hopi Point during Days 34 and 35 (see Figure 4.3) are associated with northeasterly flows which might transport Four Corners and San Juan emissions to Mexican Hat and NGS emissions to Hopi Point. The contour plot of sulfur for JD 34 hour 20 is shown in Figure 6.21.

Julian Days 39 through 44

At the beginning of the episode having the highest sulfate concentrations measured during WHITEX (Days 39–44), winds at higher levels suggest the possible influence of emissions transported from the

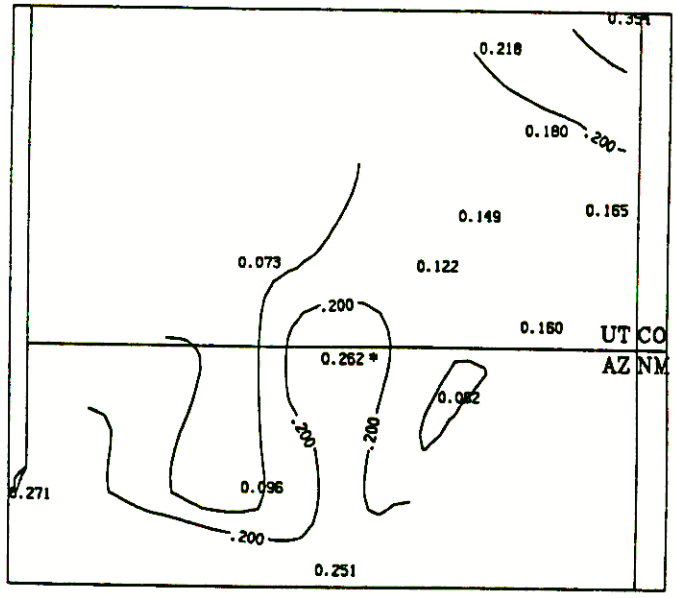

Figure 6.19: Spatial distribution of fine sulfur for JD 21 hour 8.

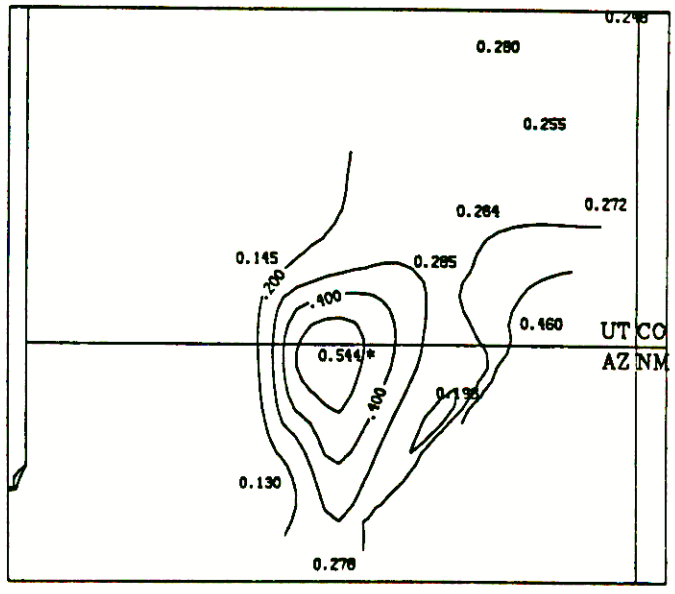

Figure 6.20: Spatial distribution of fine sulfur for JD 23 hour 8.

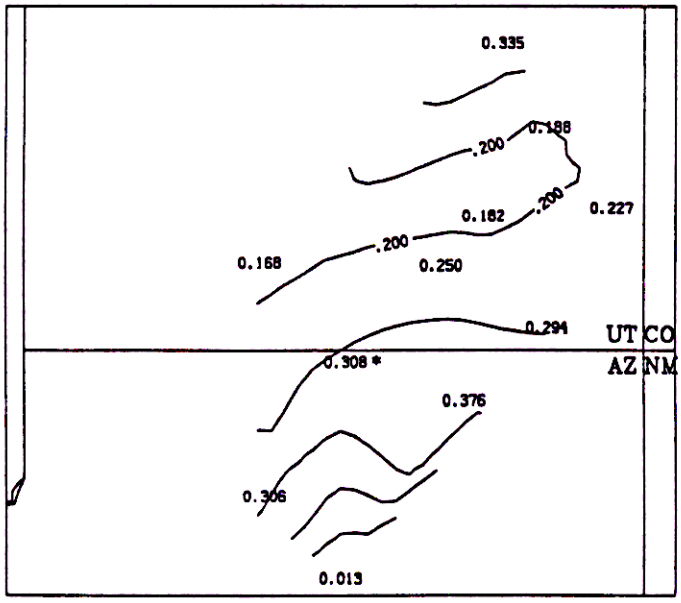

Figure 6.21: Spatial distribution of fine sulfur for JD 34 hour 20.

south and southeast from the copper smelters in southern Arizona and New Mexico. For example on JD 40 hour 8 (Figure 6.22), the concentrations are quite spatially uniform across the study area, indicating regional influences. However, later during this period, concentrations in the WHITEX region are highly nonuniform. Concentrations are highest in Page, high at Monticello, Hite, and Green River and lowest at Bryce Canyon. Winds are extremely light, variable, and sheared during this period, resulting in the dispersion of NGS emissions in all directions. The higher level winds (1000 m) are generally from the south-to-west, while lower-level winds (300 and 600 m) are more from the northeast. Thus, with such sheared winds, the NGS plume could be dispersed in opposite directions, some toward the northeast (Hite and Green River) and another portion southwestward toward Hopi Point. The contour plot of JD 42 hour 8 (Figure 6.23) shows sulfate concentrations generally decreasing outward from Page which is consistent with dispersion of NGS emissions in all directions.

Julian Days 45 through 48

The extraordinarily high winds measured on Day 45 result in a precipitous and uniform drop in regional sulfate concentrations. Compare the spatial pattern in the sulfate sulfur concentrations on JD 44 hour 8 (Figure 6.24) to that 24 hours later on JD 45 hour 8 (Figure 6.25). A buildup in sulfate begins again in Green River, Hite, Canyonlands, Monticello, and Mexican Hat on Days 47 and 48, with northeasterly flows.

Summary

This comparison of spatial and temporal trends in sulfate and meteorology shows that many sources potentially contribute to the sulfate concentrations measured during WHITEX in the study area. The non-uniformity in the spatial patterns indicates that the SO_2 sources in the region often had strong local influence on receptors nearby. NGS is a plausible contributor to many of the high sulfate

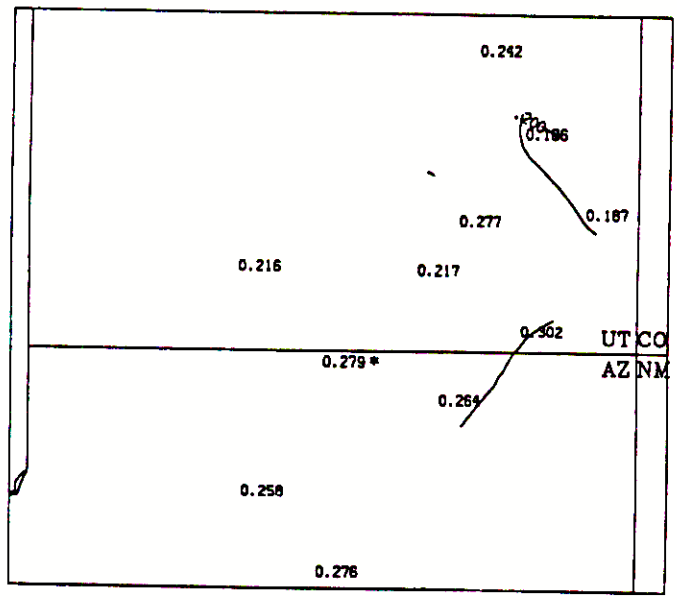

Figure 6.22: Spatial distribution of fine sulfur for JD 40 hour 8.

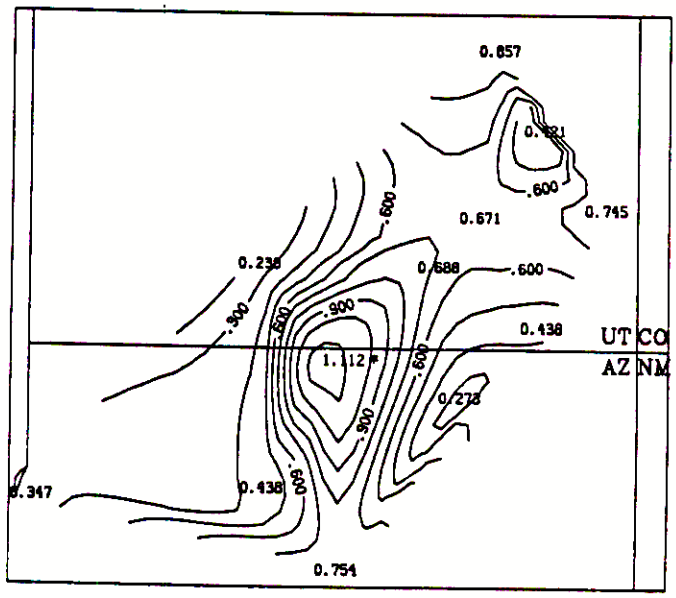

Figure 6.23: Spatial distribution of fine sulfur for JD 42 hour 8.

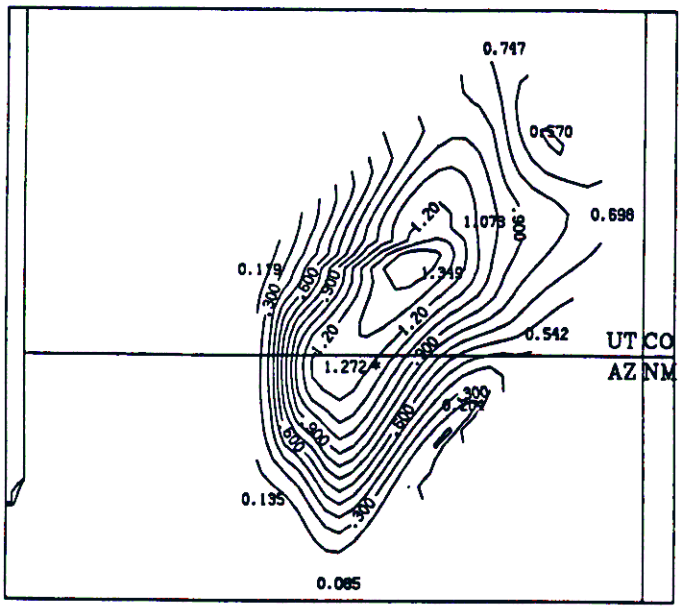

Figure 6.24: Spatial distribution of fine sulfur for JD 44 hour 8.

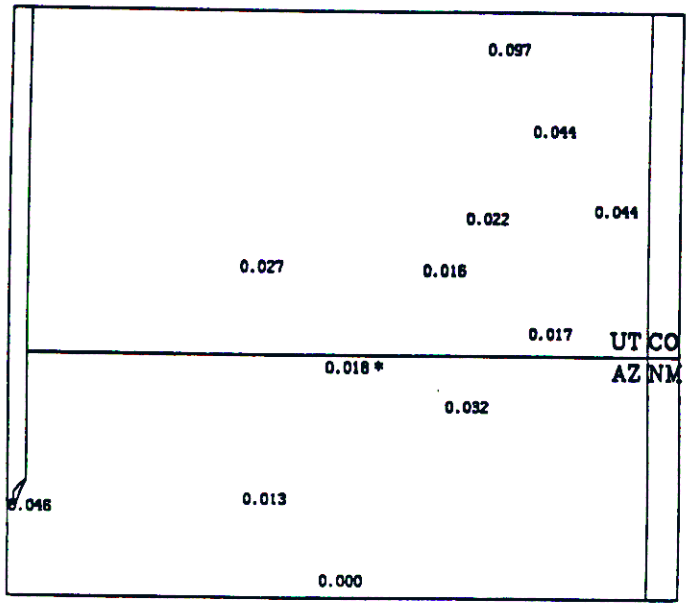

Figure 6.25: Spatial distribution of fine sulfur for JD 45 hour 8.

episodes. However, there are indications of influences from SO_x sources north of the study area and the uniformity in the sulfur concentrations during some time periods suggests some long-range transport of sulfur from more distant sources.

6.5.3 Empirical Orthogonal Function Analysis

Empirical Orthogonal Function (EOF) analysis is an analytical tool that can be used to examine the spatial patterns in the particulate concentrations. While these patterns can be determined simply by creating isopleth maps of the concentrations for each of the measurement time periods, EOF analysis has the advantage of simplifying these many maps into a few patterns (EOFs), which with knowledge of the proper weighting factors, can be linearly recombined to reproduce the observed patterns for all time periods.

The details of how the EOFs and their associated time weighting factors are determined are discussed in Appendix 6I. In principle, however, EOF analysis is simply a decomposition of a single data matrix (time by site) of pollutant concentrations into two matrices, one which is independent of time (EOF by site) and the other which is independent of location (time by EOF). Multiplication of the resulting two matrices regenerates the original time by site concentration matrix. The EOF by site matrix can be thought of as a series of isopleth maps (one for each EOF), of common concentration patterns in space, while the time by EOF matrix can be plotted as a series of time plots, also one for each EOF, which reveals the relative importance of each EOF for each sampling period. The advantage of the analysis is that while there are as many EOFs as there are sites, in general only a few of them are needed to explain most of the variance in the data. For example, in the WHITEX study, while there are 85 12-hour time periods for which we would like to examine the spatial patterns of various particulate species, only 2 EOFs are needed to explain more than 80 % of the variance in the fine sulfur data.

Both unrotated and Varimax rotated EOFs based on the centered data cross product matrix will be presented here. Varimax rotation has the property of forcing each site to load as strongly as possible onto one EOF while loading lightly on all others. It is then easier to determine which sources and meteorological conditions are most significant for each site.

Data used for EOF Analysis

The 13 WHITEX sites at which sulfur concentrations were measured are Canyonlands, Hopi Point, Bullfrog Marina, Page, Green River, Cisco, Monticello, Mexican Hat, Hite, Bryce Canyon, Navajo National Monument, Wupatki National Monument, and Meadview. See Figure 6.15 for a map of site locations.

The Meadview site was not used in the analysis because sulfur particulate samples there were collected as 24-hour averages once every three days, thus there were too many time periods with missing data. Cisco was eliminated also because there were too many missing data (48 %) there. EOF analysis allows no missing data. In addition, 6 of the 85 12-hour time periods from 1/1/87 through 2/18/87 were not used because data were missing at several sites. These time periods are Julian day (JD) 7 hour 8 and JD 7 hour 20, when data were missing at 4 sites, JD 10 hour 8, JD 11 hour 20, and JD 48 hour 20 when data were missing at 3 sites, and JD 48 hour 20 when data were missing at 6 sites.

These deletions left 79 time periods and 11 sites for use in the EOF analysis. Missing data which were preceded and followed by good data at the same site were filled by linear interpolation across time. 0.9% of the data were filled in this way. Other missing data were replaced by a distance weighted average of data at sites with non-missing data for the same time period. The weighting

Table 6.21: Eigenvalues of the sulfur correlation matrix.

Rank	Eigenvalue	Rank	Eigenvalue
1	6.70	7	0.29
2	1.57	8	0.17
3	0.65	9	0.13
4	0.59	10	0.08
5	0.46	11	0.03
6	0.33		

factor used was the inverse of the squared distance to the site with missing data. Approximately 3% of the data were replaced by this method.

Eigenvalues of Correlation Matrix

The eigenvalues of the correlation matrix which are approximately equal to the signal to noise ratio for each factor were calculated first in order to determine how many of the EOFs to retain for rotation. The results are shown in Table 6.21. Only the first 2 eigenvalues show a signal to noise ratio greater than 1. The third is only 0.65, therefore 2 EOFs were retained for the Varimax rotation.

Eigenvalues and variance explained by each EOF

The EOF analysis was then carried out on the centered data cross product matrix, which, as explained in Appendix 6I, is similar to the covariance matrix except for a constant factor of n, the number of time periods. EOFs of this matrix are desirable because the values on the maps then have units of concentration and are weighted deviations from the mean concentration at each site, thus they have physical meaning. The weights are the time factors.

The eigenvalues of each EOF as well as the variance explained by each before rotation and after Varimax rotation of 2 EOFs are shown in Table 6.22.

Discussion of unrotated EOFs

The time weighting factors for the unrotated EOFs are shown in Figure 6.26. Results for only the first 6 EOFs are shown since these are sufficient to explain more than 95% of the variance in the sulfur data. The corresponding maps for each EOF are shown in Figures 6.27, 6.28, 6.29, 6.30, 6.31, and 6.32. For site locations refer to Figure 6.15. Each value on the maps has a sign indicating a positive or negative deviation from the mean, however, the signs of the values for any given time period depend also on the sign of the time weighting factor. For example, for EOF 2, on JD 25–28, the time factor is negative, so all signs on the map (and thus the gradient) would be reversed for that time period.

When the EOFs are not rotated, the first EOF should resemble the spatial pattern which is most like a contour plot of the mean sulfur concentrations at each site. By comparing the map of unrotated EOF 1 (Figure 6.27) which explains 70 % of the variance, to a contour plot of the actual mean sulfur concentrations shown in Figure 6.33 it can be seen that this is true in general. The two maps have many similar features. The highest mean concentration, 342 ng/m^3 is at Green River, but the mean sulfur concentration at Page is only slightly lower at 318 ng/m^3. On EOF map 1, the

Table 6.22: Eigenvalues and variance explained by each EOF.

Before Rotation

Rank	Eigenvalue (ng^2m^{-6})	Variance Explained (%)	Cumulative Variance Explained (%)
1	1.6×10^7	70.1	70.1
2	2.3×10^6	10.1	80.2
3	1.2×10^6	5.4	85.6
4	8.0×10^5	3.6	89.2
5	7.0×10^5	3.1	92.4
6	5.2×10^5	2.3	94.7
7	4.7×10^5	2.1	96.8
8	3.0×10^5	1.4	98.1
9	1.9×10^5	0.9	99.0
10	1.2×10^5	0.6	99.6
11	9.7×10^4	0.4	100.0

After Varimax Rotation of 2 EOFs

Rank	Eigenvalue (ng^2m^{-6})	Variance Explained (%)	Cumulative Variance Explained (%)
1	1.3×10^7	58.4	58.4
2	4.9×10^6	21.9	80.2

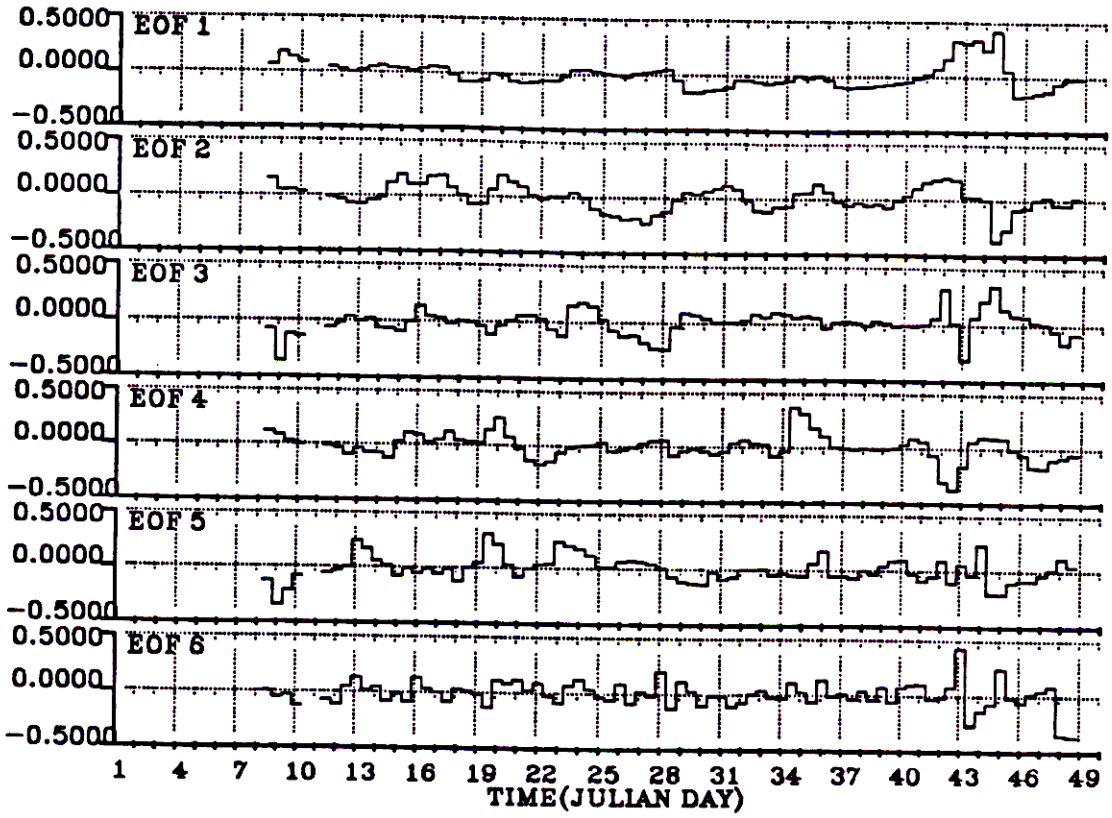

Figure 6.26: Time weighting factors for the first 6 unrotated EOFs.

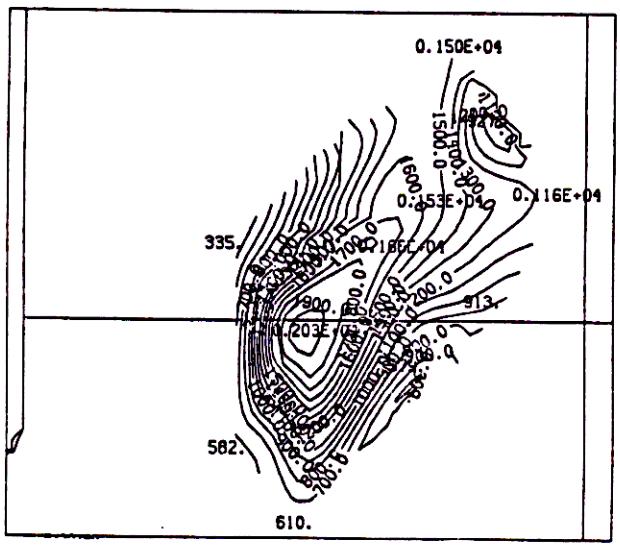

Figure 6.27: Map of unrotated EOF 1. Values on the map are weighted deviations from the mean sulfate sulfur concentrations at each site in ng/m^3.

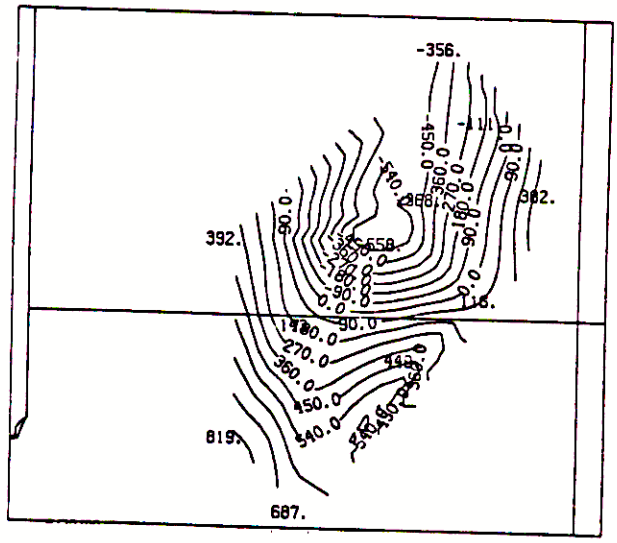

Figure 6.28: Map of unrotated EOF 2. Values on the map are weighted deviations from the mean sulfate sulfur concentrations at each site in ng/m^3.

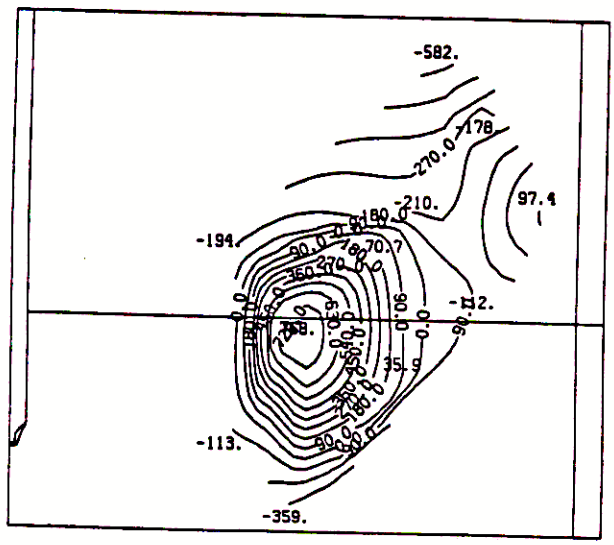

Figure 6.29: Map of unrotated EOF 3. Values on the map are weighted deviations from the mean sulfate sulfur concentrations at each site in ng/m^3.

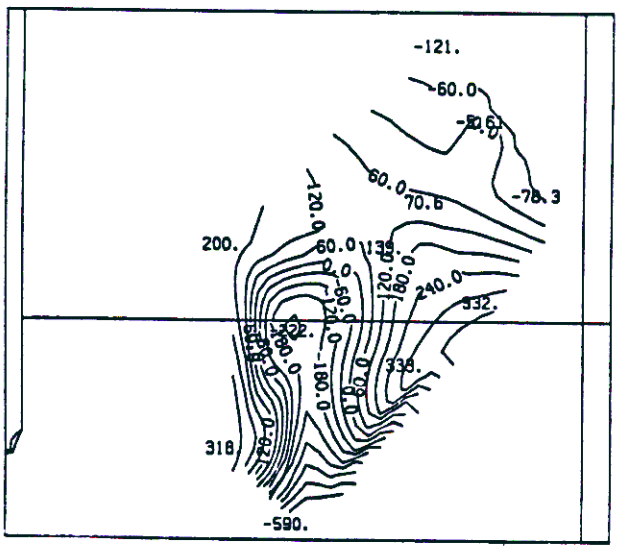

Figure 6.30: Map of unrotated EOF 4. Values on the map are weighted deviations from the mean sulfate sulfur concentrations at each site in ng/m^3.

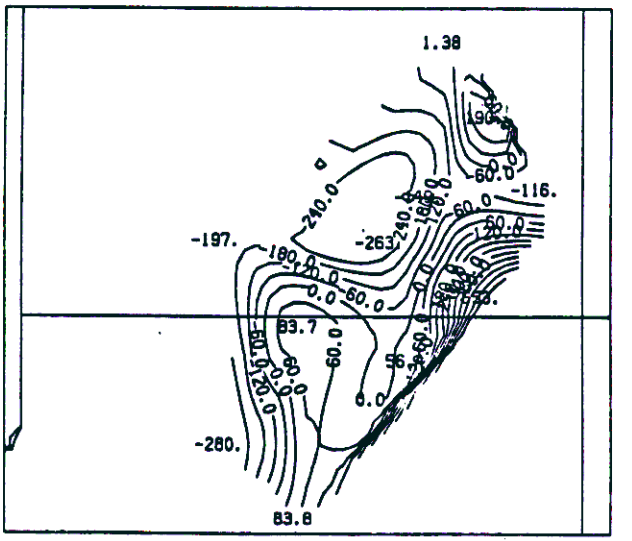

Figure 6.31: Map of unrotated EOF 5. Values on the map are weighted deviations from the mean sulfate sulfur concentrations at each site in ng/m^3.

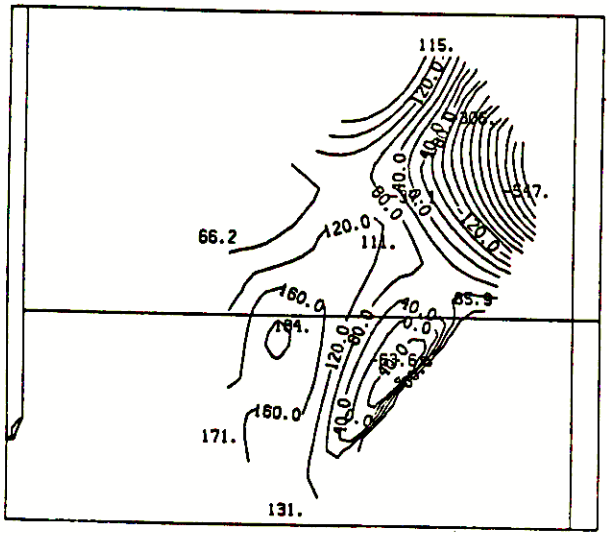

Figure 6.32: Map of unrotated EOF 6. Values on the map are weighted deviations from the mean sulfate sulfur concentrations at each site in ng/m^3.

highest loading is at Page with loadings decreasing as the distance from Page increases. The map of mean sulfur concentrations is similar, though it shows concentrations increasing again north of Hite. Because Page is the monitoring site nearest to NGS, the EOF map as well as the map of mean concentrations both suggest that NGS has a strong influence on mean sulfur concentrations in the study area. The time factors show that this EOF is most strongly weighted during the mid February episode (JD 41–44).

The succeeding EOFs are also interesting to look at since they represent other common patterns in the measured sulfur concentrations. NGS appears to be a dominant source of sulfur in EOFs 1, 3, and 4. In EOFs 5 and 6, NGS does not appear to be the dominant source, but its influence is seen by the perturbation it causes in the gradient.

Transport of sulfur into the study region from the south and southwest, perhaps indicating the copper smelters or Mohave Power Plant are sources is seen in EOF 2 when weighted positively. When EOF 2 is weighted negatively transport of sulfur into the region from sources north of the study area such as the Hunter and Huntington Power plants or the Utah power and light plants in central Utah is suggested. The second EOF is most strongly negatively weighted on February 13, when the emissions from the three northern power plants would most likely be stagnating within the Lake Powell basin. The second EOF is also strongly, negatively weighted during the period from January 24 to 28, when NGS emissions are expected to be transported to the northeast. The strongest positive weightings of the EOF occur on January 15 and 16 and February 9 to 11, when transport from the smelter region to the south was identified.

Transport into the study area from the east perhaps from the San Juan and Four Corners Plants is indicated by EOF 5. It should, however, be remembered that only the first two EOFs represent more signal than noise. Also, as seen in Table 6.22, the variance explained by each of the EOFs ranked 3 through 11 is 5% or less.

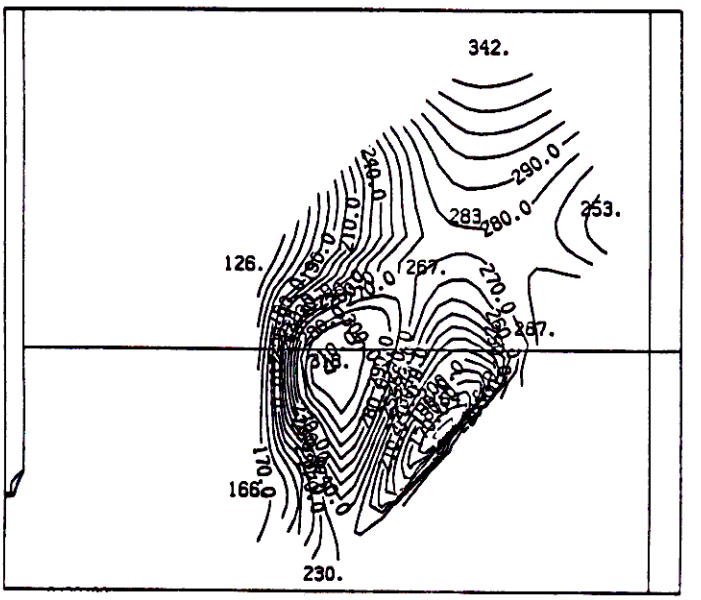

Figure 6.33: Map of mean fine sulfur concentrations

The time weighting factors (Figure 6.26) show that most sulfur episodes, are not uniquely singled out by any one of the unrotated EOFs. Sulfur concentrations are seen to be a linear combination of several patterns.

Discussion of the rotated EOFs

The rotated EOFs are potentially more useful for determining the source areas which may influence each receptor since each site should load strongly to only one factor.

Since the eigenvalues of the correlation matrix indicate that only the first 2 EOFs have a signal to noise ratio greater than 1, the Varimax rotation was done with only these 2 factors. The two resulting maps, are shown in Figures 6.35 and 6.36. The time factors are shown in Figure 6.34.

EOF 1, associated with 58% of the variance, indicates dispersion of sulfur outward from NGS. A preferred transport direction appears to be to the north and northeast of Page. However, sulfur concentrations are greater than the means at all monitoring sites in the study region. This EOF is weighted most strongly during the February episode (JD 42–45).

EOF 2 (32 % of the variance) also suggests that NGS is the dominant source of sulfur for time periods when this EOF is weighted positively, although the preferred transport direction appears to be southwestward from Page. Transport of sulfur into the study region from the east is also indicated. This EOF is weighted most strongly on JD 40–45 and 13–18.

The time factors show that during the major sulfate episode (JD 40–45) both patterns were weighted strongly, The JD 13–17 episode is attributed solely to EOF 2. The JD 25–28 episode is a combination of a positive contribution from EOF 1 and a negative contribution from EOF 2.

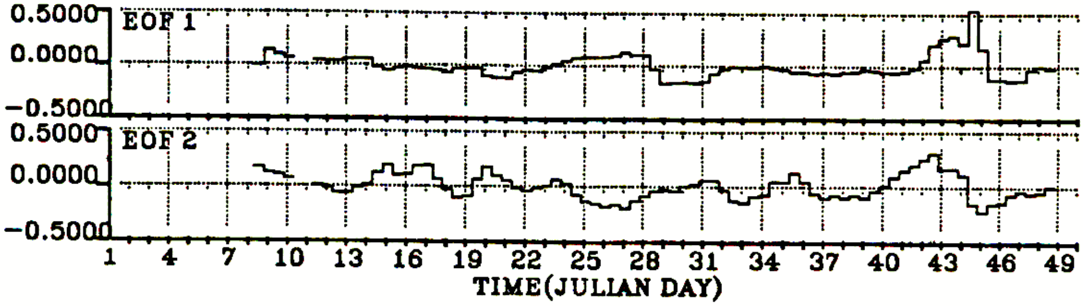

Figure 6.34: Time weighting factors for 2 rotated EOFs.

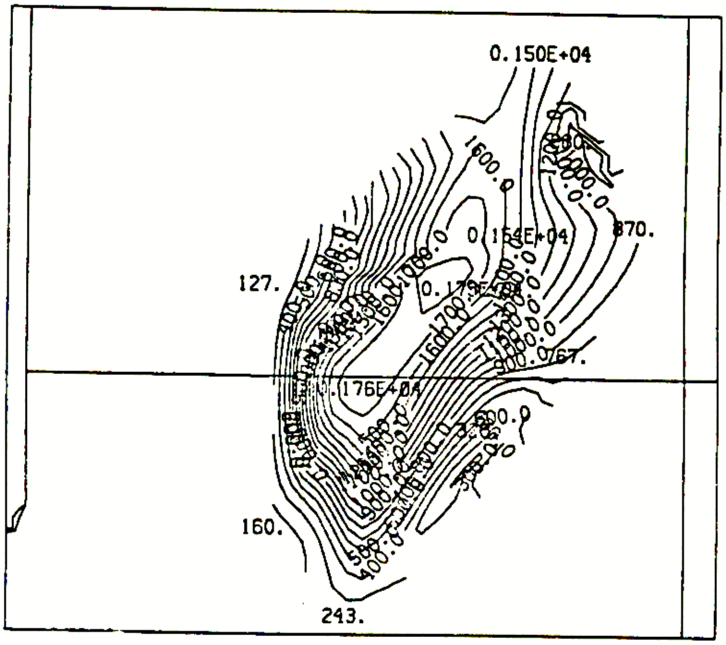

Figure 6.35: Map of rotated EOF 1 when 2 EOFs are rotated. Values on the map are weighted deviations from the mean sulfate sulfur concentrations at each site in ng/m^3.

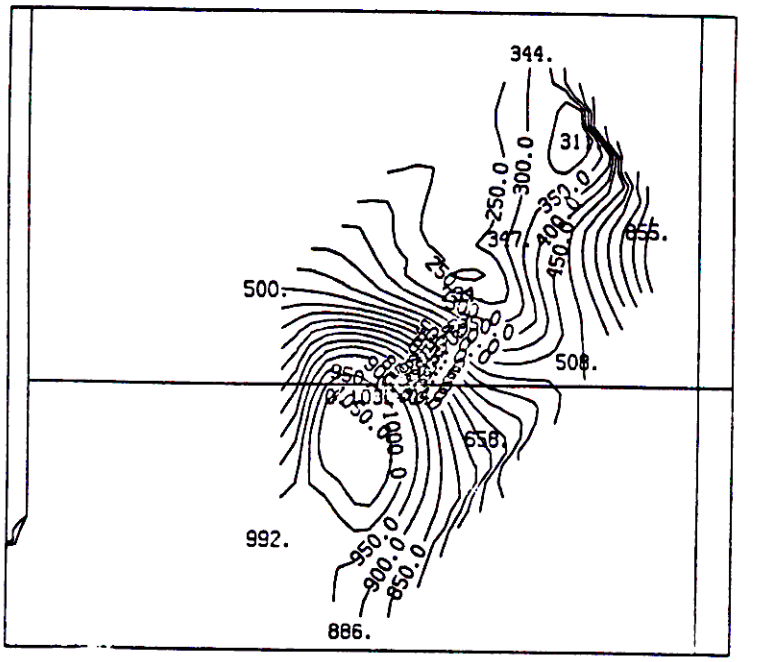

Figure 6.36: Map of rotated EOF 2 when 2 EOFs are rotated. Values on the map are weighted deviations from the mean sulfate sulfur concentrations at each site in ng/m^3.

6.6 Assessment of Quantitative Attribution Techniques

There are a number of receptor oriented models that have been used to attribute primary aerosols to their sources while very few attempts have been made to apportion secondary aerosols using receptor oriented techniques. The chemical mass balance (CMB) model has historically been the most popular receptor oriented model. It essentially uses the relative ratios of natural or man-made tracers at the sources and receptor locations to apportion primary species at one point in time. Tracer mass balance regression (TMBR) on the other hand uses the variation of trace material across time to achieve apportionment of primary or secondary aerosols. Finally, the differential mass balance (DMB) approach uses trace material to establish dispersion factors but calculates the effects of deposition and oxidation explicitly. Assumptions, limitations,and method of calculating uncertainties for each of these model is covered in Appendices 6D, 6B, and 6C. Also presented in Appendix 6A is the recently formulated general mass balance model (GMB). It is an attempt to combine the tracer mass balance regression model, the chemical mass balance model and differential mass balance approach into one umbrella formalism. This formalism allows for a straight forward exploration of assumptions and deviation from assumptions that are required to carry out the apportionment calculations.

Each of the subsequent sections present the attribution calculation along with uncertainty analysis for each of receptor oriented approaches.

6.6.1 Tracer Mass Balance Regression

Tracer mass balance regression (TMBR) is one simplification of the general mass balance model. The equations, assumptions and possible deviations from assumptions associated with TMBR are